Landslides
DOI 10.1007/s10346-008-0137-0
Received: 24 July 2007
Accepted: 8 June 2008

Adam B. Prochaska · Paul M. Santi · Jerry D. Higgins · Susan H. Cannon

A study of methods to estimate debris flow velocity

Abstract Debris flow velocities are commonly back-calculated from superelevation events which require subjective estimates of radii of curvature of bends in the debris flow channel or predicted using flow equations that require the selection of appropriate rheological models and material property inputs. This research investigated difficulties associated with the use of these conventional velocity estimation methods. Radii of curvature estimates were found to vary with the extent of the channel investigated and with the scale of the media used, and back-calculated velocities varied among different investigated locations along a channel. Distinct populations of Bingham properties were found to exist between those measured by laboratory tests and those back-calculated from field data; thus, laboratory-obtained values would not be representative of field-scale debris flow behavior. To avoid these difficulties with conventional methods, a new preliminary velocity estimation method is presented that statistically relates flow velocity to the channel slope and the flow depth. This method presents ranges of reasonable velocity predictions based on 30 previously measured velocities.

Keywords Debris flow · Velocity · Superelevation · Mitigation · Design

Introduction

A debris flow is "a mass movement that involves water-charged, predominantly coarse-grained inorganic and organic material flowing rapidly down a steep, confined, preexisting channel" (VanDine 1985). Debris flows are hazardous due to their poor predictability, high impact forces, and their ability to deposit large quantities of sediment in inundated areas. Debris flow mitigation structures may be required to minimize the risk to developments on alluvial fans. Debris flow velocity is an important factor in the design of mitigation structures because it influences the impact forces, run-up, and superelevation of the flow. Debris flow velocities are conventionally back-calculated from previous superelevation events (Johnson 1984) or predicted using flow equations (Lo 2000). A velocity back-calculation from a superelevation event requires an estimate of the bend's radius of curvature, which is a subjective concept for a natural channel but may be reasonably estimated. A velocity prediction using a flow equation requires the selection of an appropriate rheological model and its material property inputs.

This study investigates the difficulties associated with the use of these conventional velocity methods. Errors associated with the estimation of radius of curvature through different methods are examined, as is the problem with estimating rheological properties through laboratory tests. Velocity, flow depth, and channel slope trends along the paths of debris flows are also investigated, and we propose a new method for preliminary debris flow velocity estimations that avoids the abovementioned difficulties. This method statistically relates flow velocity to the channel slope and the depth of flow based on 30 previously measured velocities from the technical literature.

Background

Velocity back-calculations

In order to estimate the velocity of a past debris flow, a superelevation event is required. Superelevation refers to the difference in surface elevation, or banking, of a debris flow as it travels around a bend. Higher velocities result in increased banking. If the bend geometry is known, flow velocity can be estimated from superelevation or vice versa. An existing superelevation can be measured from bank levees to estimate the velocity of the flow that formed them. The required height of deflection structures can be estimated by predicting the superelevation from a flow with a given velocity. Based on the results of large-scale flume experiments, back-calculation using superelevation may presently be the most accurate way to estimate debris flow velocity (Iverson et al. 1994). The most commonly referenced method for making this estimation is the forced vortex equation (Chow 1959; Henderson 1966; Hungr et al. 1984; Johnson 1984), which equates fluid pressure to centrifugal force (McClung 2001):

$$v = \sqrt{\frac{R_c g}{k}\frac{\Delta h}{b}} \tag{1}$$

where:

- v mean flow velocity,
- R_c the channel's radius of curvature,
- g acceleration of gravity,
- Δh superelevation height (Fig. 1),
- k correction factor for viscosity and vertical sorting, and
- b the flow width (Fig. 1).

The banking angle (β) can be measured instead of measuring b and Δh, where $\beta = \tan(\Delta h/b)$. In order to account for the slope-normal component of gravity, g should be replaced with g^* if the channel slope is greater than 15°, where $g^* = g\cos\theta$, and θ is the channel slope (Johnson 1984).

Equation 1 assumes that flow is subcritical, the radius of curvature is equal for all streamlines, and every streamline's velocity is equal to the mean flow velocity (Pierson 1985). Equation 1 was originally derived for water, and thus, the correction factor k is sometimes applied to account for the viscosity and vertical sorting of particles within debris flows (Hungr et al. 1984). Different studies suggest different values for k in order to match experimental superelevations to theoretical values. Suwa and Yamakoshi (2000) mention that k is usually greater than or equal to 1. VanDine (1996) stated that k may vary between 1 and 5. Hungr et al. (1984) reported that k may vary

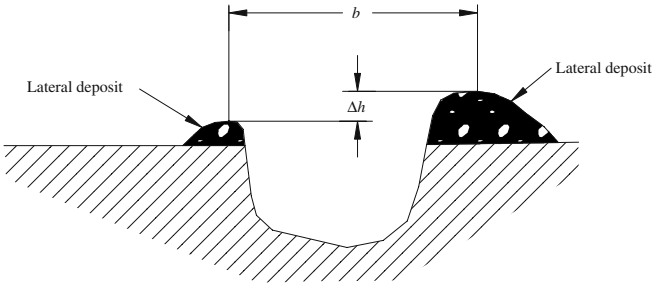

Fig. 1 Flow width (b) and superelevation height (Δh) in a superelevated cross-section (after Johnson 1984)

between 2.5 and 5. Chen (1987) reported that k may be as high as 10, and its value may depend on bend geometry and debris flow material properties. O. Hungr (5 January 2007, personal communication) now believes that the correction factor is unity except for cases of very sharp bends where shock waves develop. Other references to the forced vortex equation in the technical literature do not mention the use of a correction factor.

McClung (2001) believed that the fluid principles used to derive the forced vortex equation (Eq. 1) were not appropriate for frictional materials such as avalanches and debris flows. Instead, he derived a superelevation equation that accounts for basal friction and passive earth pressures. For a symmetrical triangular channel,

$$\frac{v^2}{R_c g*} = \frac{y}{B} + \frac{\Delta y}{B} - \frac{yK_p \cos^2 \psi \cos 2\psi}{B} + \mathrm{sgn}(v_s)\mu \qquad (2)$$

where:

v	flow velocity,
R_c	radius of curvature,
g^*	slope-normal component of gravity, as described above,
y	flow depth in channel center,
B	half-width of flow,
Δy	superelevation elevation above the flow depth in channel center,
K_p	passive earth pressure coefficient,
ψ	channel side slope,
$\mathrm{sgn}(v_s)$	−1 for downward basal slip or +1 for upward basal slip, and
μ	effective basal friction coefficient.

Additional uncertainties in this equation beyond those in the forced vortex equation exist in estimations of an effective dynamic internal friction angle, an effective frictional coefficient, and the direction of basal slip. More equations for relating velocity to superelevation are presented by Apmann (1973).

For the superelevation equations described above, an estimate of the channel radius of curvature is required. The technical literature frequently refers to the radius of curvature of the center of a channel around a bend, but little guidance is given as to how it should be estimated. The radius of curvature can be mathematically calculated at any point if a flow path is represented by a function that can be differentiated twice (Thomas and Finney 1984):

$$R_c = \frac{\left[1 + (dy/dx)^2\right]^{3/2}}{\left|d^2y/dx^2\right|}. \qquad (3)$$

Since a bend in a natural channel is not a perfect circle, but rather has a varying curvature, estimation of the radius of curvature will depend on where and how the curve is examined. Reneau and Dietrich (1987) imply that they estimated the radius of curvature by surveying five channel cross-sections perpendicular to the direction of flow, with spacings of approximately 10 m. Williams (1986) estimated the radii of curvature of river meanders by subjectively overlaying best-fit circular arcs on the centerlines of the meander loops. Because of the subjectivity in this method, he found that radii of curvature estimates between any two investigators could vary by 25%. Reneau and Dietrich (1987) found that a varying radius of curvature around a bend made it difficult to estimate consistent velocities with the forced vortex equation. The subjectivity in estimating a radius of curvature can be reduced by computing it along a digitized channel's centerline using Eq. 3 and finite differences for the spatial derivatives (J. Kean, 1 August 2007, written communication), but such sophisticated methods are yet to be reported in the debris flow literature.

Other uncertainties with the use of superelevation equations include differences that may exist between the post-flow channel alignment and the alignment at the time of the superelevation event, erroneous superelevation values due to splashing, and whether the flow characteristics match the equation assumptions presented above. However, the main focus of this paper is the variability associated with the estimation of R_c through different investigation techniques.

Velocity predictions

A limitation of Eqs. 1 and 2 is that they require the occurrence of a debris flow event in order to estimate the velocity; these equations cannot be used to predict a debris flow velocity before an event occurs. However, several flow equations exist that can be used to predict a debris flow velocity; many of these equations are presented by Lo (2000), Rickenmann (1999), and Rickenmann and Koch (1997). These equations take the general form of:

$$v = a \times h^b S^c \qquad (4)$$

where:

v	velocity,
a	factor that incorporates debris and channel properties,
h	flow depth,
S	sine of the channel angle, and
b and c	exponents that depend on the assumed flow characteristics.

Equations of this form (Eq. 4) are based on fluid dynamics assumptions for steady, uniform flow in shallow channels. However, these equations are also used to approximate the velocities of debris flows, which can be unsteady, non-uniform, and occur in steep channels. The Bingham laminar flow equation (Lo 2000; Rickenmann and Koch 1997) is one such velocity equation and takes the form:

$$v = \frac{\rho_d g h^2 S}{k\mu_B}\left(1 - 1.5\frac{\tau_B}{\tau_o} + 0.5\frac{\tau_B^3}{\tau_o^3}\right) \qquad (5)$$

where:

ρ_d debris density,
g acceleration of gravity,
h and S as defined in Eq. 4,
k 3 for a wide rectangular channel, 5 for a trapezoidal channel, and 8 for a semicircular channel,
μ_B Bingham viscosity,
τ_B Bingham yield stress, and
τ_o basal shear stress.

Some researchers believe that because of the complexity of debris flows in both space and time, their motion cannot be represented by a single rheological equation (Iverson 2003). Others advocate a simple model because of the inherent complexity of these flows (O'Brien 1986). Lo (2000) and Rickenmann and Koch (1997) recommend the use of Newtonian turbulent flow equations, but the two sources report using vastly different roughness and frictional coefficients in order to obtain fits to their datasets. Other researchers advocate the use of Bingham models (Johnson 1984), especially for muddy debris flows (O'Brien 1986). The Bingham laminar flow equation (Eq. 5) is most applicable to flows that can be modeled as having a yield strength and a linear relationship between shear rate and shear stress (Pierson and Costa 1987). Although inputs to the Bingham flow equation may also be quite variable (Costa 1984; Iverson 1997) and may not be able to accurately model the complexity of debris flows (Iverson 2003), simple laboratory tests can be used to estimate these debris properties (Johnson and Martosudarmo 1997; Pashias and Boger 1996). However, Bingham parameters are dependent on the maximum particle size of the debris flow material that is sampled and tested.

Data sources

This study investigated the difficulties associated with both back-calculating and predicting debris flow velocities. Much of the data used for this study came from field measurements of channel cross-sections (Santi et al. 2006). Channel cross-sections were measured using a slope profiler (Gartner 2005; Keaton and DeGraff 1996; Santi 1988) following debris flow events from recently burned drainage basins (Gartner 2005). A slope profiler consists of a wood crossbar with two legs and an angle finder; the angle finder reports the slope of the ground surface between the two legs. By taking sequential angle measurements at a cross-section and trigonometrically converting the measured angles to x and y coordinates, a profile of each cross-section was developed. Cross-sections were spaced at 15- to 90-m intervals along the entire channel length. At each cross-section, it was also noted which slope profiler intervals corresponded to levee deposits, muddy veneer deposits, channel incision, bedrock, and the natural slope. The channel slope and azimuth were also recorded for each cross-section.

Topographic maps (1:24,000-scale) and airphotos (1:15,000- and 1:8,000-scale) were used to estimate channel radii of curvature at cross-section locations.

Velocity, channel characteristic, and material property data were obtained from the technical literature to investigate the appropriateness of conventional velocity back-calculation and prediction techniques and also to investigate velocity patterns along flow paths. Specific data sources are referenced in subsequent sections and are summarized in Table 1. This data summary suggests that debris flow events analyzed within the technical literature are primarily large events, and thus, the dataset may be biased towards higher (more conservative) velocities.

Field estimations of R_c

Methods

To estimate the ease with which a bend's radius of curvature can be approximated in the field, an investigation was performed along a channel bend with superelevated debris flow deposits in Kroeger Canyon, Durango, Colorado (Gartner 2005). Eight cross-sections were measured around the bend at approximately 6-m spacings. At each cross-section, the azimuth normal to the channel orientation was measured. Multiple radii of curvature were calculated between various pairs of cross-sections by relating arc lengths to the included angles:

$$L = 2\pi R_c \times \frac{\theta}{360} \tag{6a}$$

$$R_c = \frac{360L}{2\pi\theta} \tag{6b}$$

where:

R_c radius of curvature,
L channel length (arc length) between the two cross-section, and
θ angular difference (degrees) between the two cross-section azimuths.

Radii of curvature between different sections were calculated with Eq. 6b using channel lengths between 6 and 42 m.

Results

The calculated radii of curvature versus the spacings between the cross-sections are shown in Fig. 2. Positive and negative radii correspond to clockwise and counterclockwise curvature, respectively. The analyzed arc length represents the channel length between the pair of analyzed cross-sections. Multiple data points were obtained for each analyzed arc length by investigating pairs of cross-sections at different positions around the bend. Different analyzed arc lengths were obtained by skipping cross-sections between those used in the investigated pair.

Discussion

As the analyzed arc lengths in Fig. 2 increase, the calculated radii of curvature begin to stabilize at a consistent value of approximately −100 m (counterclockwise curvature with R_c=100 m). However, considerable scatter exists between the radii of curvature calculated from arc lengths shorter than approximately 25 m. Scatter exists for each given arc length, which indicates that the estimation of the radii of curvature is dependent upon the location along the arc at which it is measured. Estimated radii of curvature were both positive and negative (clockwise and counterclockwise curvature, respectively), which indicates that this estimation method is very sensitive to the measured azimuths of the cross-sections. It appears as if a field investigation method concentrates on local channel irregularities and does not allow for the observer to get a good overall picture of the curve, as an airphoto or map would.

Table 1 Summary of data obtained from the technical literature

Reference	Event/Location	Event notes	Data used from reference	Data acquisition methods
Supercritical versus subcritical flows (Fig. 10)				
Arattano et al. (1997)	Moscardo Torrent, Italy	10 events from 1990 to 1994	Velocity and flow depth	Ultrasonic sensors
Jackson et al. (1989)	Cathedral Mountain, British Columbia	29 August 1984 (87,000 m^3)		Measured channel cross-sections, velocities back-calculated from superelevation
Jan et al. (2000)	Jiangjia Gulley, China	8 waves from a debris flow in 1974		Measured at observation station
Jordan (1994)	14 events in British Columbia			Measured channel cross-sections, velocities back-calculated from superelevation
McArdell et al. (2003)	Illgraben torrent, Switzerland	28 June 2000 (35,000 m^3)		Radar and video analysis
Santi (1988)	Layton, Utah	12,000 m^3		Measured channel cross-sections, velocities back-calculated from superelevation
Tropeano et al. (2003)	Bioley torrent, Italy	92,000 m^3		Measured channel cross-sections, velocities back-calculated from superelevation
Laboratory-measured Bingham properties (Fig. 11)				
Hamilton and Zhang (1997)	Jiang-Jia Gulley, China	47 samples from 9 events in 1974 and 1975	Yield strength and viscosity	Laboratory analyses
	U.C. Davis flume, California	7 samples		Laboratory analyses
Johnson and Martosudarmo (1997)	Laboratory-prepared water/sand and slurry/sand mixtures	15 to 48 % solids by volume		Rolling-sleeve viscometer
Locat (1997)	Canadian clays and clayey silts			HAAKE Rotovisco 12
Soule (2006)	Samples of debris-flow deposits from Georgetown and Glenwood Springs, Colorado	Tested samples containing particles up to 25.4 mm (1 in.)		Flume box, rolling-sleeve viscometer, inclined plane, slump test
Field back-calculated Bingham properties (Fig. 11)				
Bertolo and Wieczorek (2005)	Yosemite Valley, California	6 events	Yield strength and viscosity	Back-calculated from numerical modeling
Hungr et al. (1984)	British Columbia and Japanese data	15 events	Viscosity	Best-fit to velocity – depth data using Newtonian Laminar flow equation
Johnson (1984)	Surprise Canyon, California	500,000 m^3	Yield strength	Estimated from deposit thickness and sizes of transported clasts
Jordan (1994)	8 events from western United States, New Zealand, and Philippines	Mean value used when range was reported	Yield strength and viscosity	Review of published data
	11 events in British Columbia	Mean value used when range was reported	Yield strength and viscosity	Estimated from deposits and velocities back-calculated from superelevations
Marina and Giuseppe (2007)	Molise Region, Italy	Hypothetical situations based on potential source areas and the active alluvial fan	Yield strength and viscosity	Back-calculated from numerical modeling
Rickenmann and Koch (1997)	Kamikamihori valley, Japan		Yield strength and viscosity	Back-calculated from numerical modeling
Soule (2006)	Georgetown and Glenwood Springs, Colorado debris flows		Yield strength	Estimated from deposit thicknesses
Velocity versus position along flow path (Figs. 12 and 13)				
Arattano (2003)	Moscardo Torrent, Italy	22 June 1996	Velocity	Ultrasonic and seismic sensors
Bertolo and Wieczorek (2005)	Yosemite Valley, California		Velocity	Back-calculated from superelevation
Curry (1966)	Mayflower Gulch, Colorado	18 August 1961 (17,000 m^3)	Velocity	Eyewitness
DeGraff (1997)	Pilot Ridge, California	2 January 1997 (460 m^3)	Velocity	Back-calculated from run-up and superelevation

Table1 (continued)

Reference	Event/Location	Event notes	Data used from reference	Data acquisition methods
Jackson (1979); Jackson et al. (1989)	Cathedral Mountain, British Columbia	6 September 1978 (136,000 m^3)	Velocity	Eyewitness
Jackson et al. (1989)	Cathedral Mountain, British Columbia	29 August 1984 (87,000 m^3)	Positions of 5 velocity estimates	Back-calculated from superelevations
Jakob et al. (1997)	Pierce Creek and Hope Creek, British Columbia	November 1995 (63,000 and 50,000 m^3)	Velocity	Back-calculated from superelevations
Jakob et al. (2000)	Hummingbird Creek, British Columbia	11 July 1997 (92,000 m^3)	Positions of 9 velocity estimates	Back-calculated from superelevations
Johnson (1984)	Surprise Canyon, California	500,000 m^3	Velocity	Back-calculated from superelevation
Meyer and Wells (1997)	Twelve Kilometer, Wyoming	9 July 1989 (8,500–14,800 m^3)	Velocity	Back-calculated from run-up
Meyer et al. (2001)	Jughead Creek, Idaho	January 1997 (14,600 m^3)	Velocity	Back-calculated from run-up and superelevation
Nasmith and Mercer (1979)	Gulley #1, Port Alice, British Columbia	15 December 1973 (22,000 m^3)	Velocity	Eyewitness
Santi (1988)	Layton, Utah	12,000 m^3	Positions of 7 velocity estimates	Back-calculated from superelevations
h^2S versus position along the flow path (Fig. 14 and Table 2)				
Gartner 2005	Tributary 2, Santaquin, Utah	3,700 m^3	Flow depth and channel slope	Slope-profiler measurements of channel cross-sections
	Tributary 3, Santaquin, Utah	6,200 m^3		
	Tributary 4, Santaquin, Utah	7,000 m^3		
	Tributary 5, Santaquin, Utah	3,000 m^3		
	Tributary 6, Santaquin, Utah	5,300 m^3		
	Elkhorn, Durango, Colorado	5,300 m^3		
	Kroeger, Durango, Colorado	15,800 m^3		
	Woodard, Durango, Colorado	6,500 m^3		
	Devore, southern California	22,500 m^3		
	El Capitan I, southern California	450 m^3		
	Lytle Creek W, southern California	10,400 m^3		
	Waterman N North, southern California	204,000 m^3		
	Water Tank, southern California	2,200 m^3		
Velocity versus h^2S (Fig. 15)				
Jackson et al. (1989)	Cathedral Mountain, British Columbia	29 August 1984 (87,000 m^3)	Velocity, flow depth, and channel slope	Measured channel cross-sections, velocities back-calculated from superelevation
Jordan (1994)	14 events in British Columbia			
Santi (1988)	Layton, Utah	12,000 m^3		
Tropeano et al. (2003)	Bioley torrent, Italy	92,000 m^3		

Figure 3 depicts an example of how both clockwise and counterclockwise curvatures can be obtained from the same bend. If the observer is within a deeply incised channel and a wide extent of the bend cannot be viewed, the azimuth normal to the flow direction may be incorrectly referenced from the orientation of the post-debris-flow stream thalweg. In Fig. 3, cross-sections (XS) 1 and 2A are both correctly orientated normal to the flow direction, and analysis of these cross-sections would accurately provide clockwise curvature. Cross-section 2B is oriented normal to the thalweg but not to the flow direction, and analysis of cross-sections 1 and 2B would result in a large-radius counterclockwise curvature.

R_c variations for different lengths of channel bends

Methods

Although the radius of curvature at the point of superelevation (apex of the bend) is required, circle overlaying techniques cannot be used to identify the radius at a single point. Instead, the radius must be estimated by examining the curvature of a length of the channel. To investigate how estimated radii of curvature varied as the examined lengths of channel bends changed, radii were measured on 1:24,000-scale topographic maps image-referenced into AutoCAD. Radii were measured on circular arcs fit to sets of points marked on the bend. The first marked point was at a location of maximum curvature within the debris-flow-producing channels. Points were also placed 30, 60, and 90 m upstream and downstream of the points of maximum curvature.

AutoCAD's drawing function was used to place circles through three points: the point of maximum curvature and one point on either side of it spaced at 30, 60, or 90 m. The radii of curvature for each circle were identified by viewing the circle properties. The following basins were investigated: tributaries 2, 3, 4, 5, and 6 from Santaquin, Utah (Gartner 2005; McDonald and Giraud 2002) and Kroeger and Woodard Canyons from Durango, Colorado (Gartner 2005).

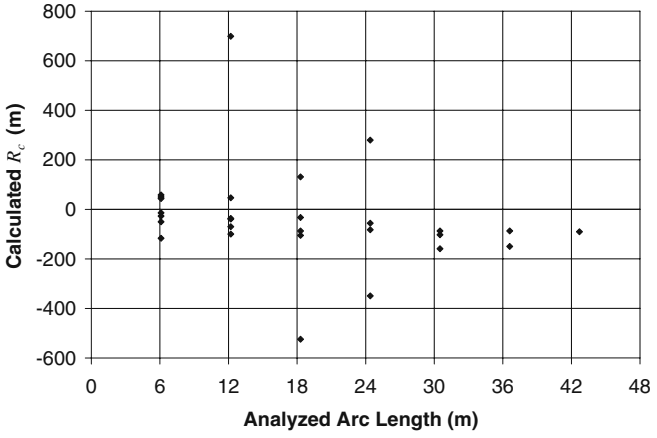

Fig. 2 Calculated R_c versus the analyzed length of arc

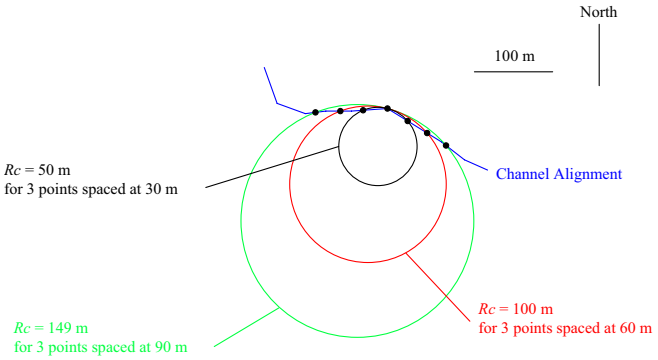

Fig. 4 Example of how a calculated radius of curvature changes as the investigated extent of the channel changes

In addition to estimating radii of curvature from a circle fit to three points, the use of a second-order polynomial was also investigated. The coordinates of the three points along the bends were identified using AutoCAD, and second-order polynomials were fit to these points. The polynomials were differentiated twice and radii of curvature were calculated using Eq. 3.

Results

Figure 4 depicts an example of how a bend's radius of curvature, as estimated by a circle fit to three points along the channel, changes as the investigated length of the channel changes.

A summary of all the analyzed cross-sections is presented in Fig. 5. In Fig. 5, the *y*-axis depicts the radii of curvature calculated from a circle with 60 or 90-m point spacings normalized by (divided by) the radii of curvature obtained from a circle when 30-m point spacings were used.

Discussion

Figure 5 shows that larger radii of curvature resulted when longer extents of curves were examined. This phenomenon is magnified for tighter bends. Thus, an estimated radius of curvature for a natural channel will depend upon what extent of the bend is examined. As the examined length of channel decreases, the estimated radius will approach that for the singular point of superelevation. Therefore, to analyze the shortest possible channel length, the largest scale, highest resolution media available should be used.

It appears that for radii of curvature greater than approximately 200 m, or more than twice the largest point spacing of 90 m, less dependence on point spacing is shown. However, radii of curvature used to back-calculate velocities reported in the technical literature are typically less than 100 m (Bertolo and Wieczorek 2005; Chou et al. 2000; Cui et al. 2005; Jackson et al. 1989; Jakob et al. 1997; Johnson 1984; Jordan 1994; Santi 1988).

For this study, the arbitrary point spacings of 30, 60, and 90 m were chosen to systematically analyze the changes in estimated radii for various curves as the analyzed curve segments increased. In practice, judgment would be required to select the locations of representative points on a case-by-case basis.

The calculation of radii of curvature from polynomials was impractical. The accuracy of the differentiation procedure was highly dependent upon the number of significant figures within the polynomial coefficients. In order to obtain realistic radii from Eq. 3, more accuracy was required than could reasonably be expected from 1:24,000-scale topographic maps.

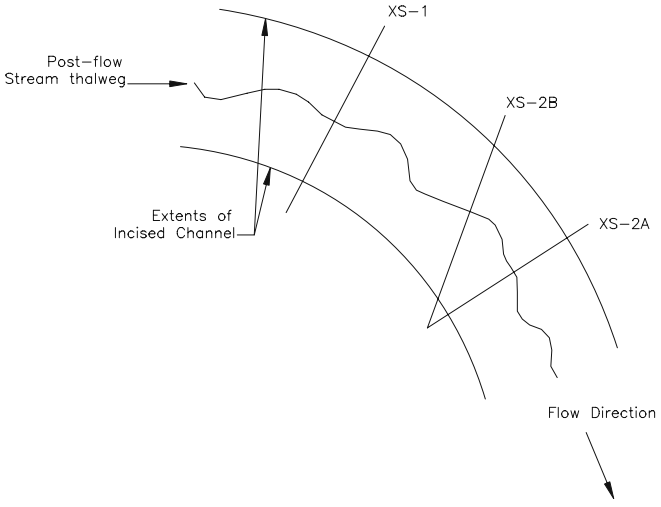

Fig. 3 Example of how clockwise and counterclockwise curvature can be measured from the same bend

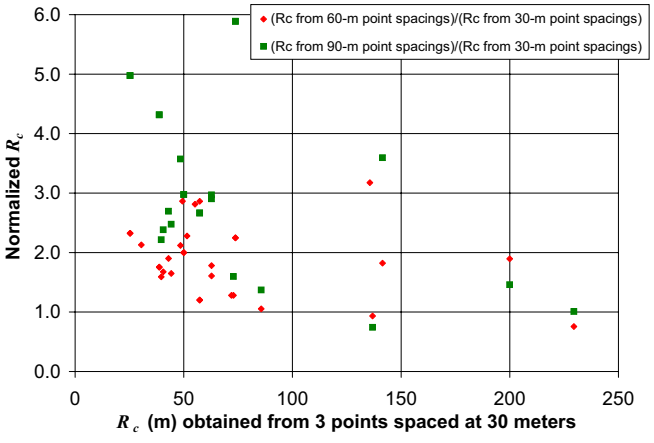

Fig. 5 Normalized calculated radii of curvature from a fitted circle versus the radii of curvature calculated from a circle fit to three points spaced at 30 m

R_c variations with different scales of investigated media

Methods

To investigate how radii of curvature varied for different scales of investigated media, a debris flow in Layton, Utah (Santi 1988) was analyzed using a 1:24,000-scale topographic map and 1:15,000-scale and 1:8,000-scale airphotos. The following cross-sections from Santi (1988) were examined: 3, 13, 15, 18, 28, and 35. The map and airphotos were image-referenced into AutoCAD. At each cross-section location, circles were overlaid upon the channel in radii increments of 15 m in order to estimate the maximum and minimum probable radii of curvature. The radius of curvature for each cross-section was taken as the average of the maximum and minimum. This process was repeated using all three scales of media.

Results

Figure 6 shows an example of the maximum and minimum radii of curvature estimated for cross-sections 13, 15, and 18 of the Layton, Utah debris flow (Santi 1988). The same aerial extent is presented on the three media shown in Fig. 6, and the displayed media are proportional to their original scales.

A summary of all the data is presented in Fig. 7. In Fig. 7, the *y*-axis depicts the average radii of curvature estimated from different scale media normalized by the radii estimated from the 1:8,000-scale airphoto.

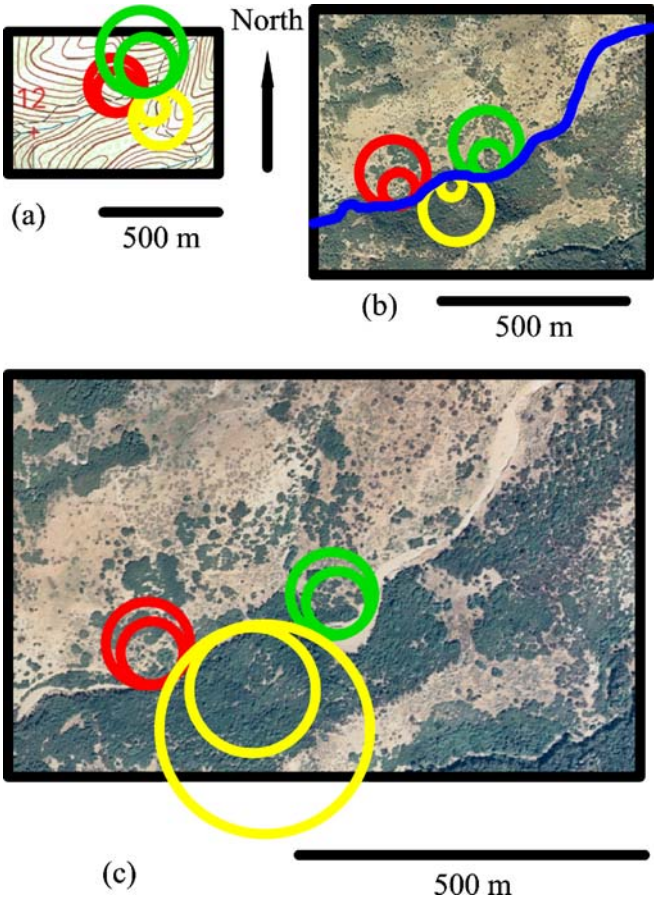

Fig. 6 Examples of maximum and minimum radii of curvature identified using a 1:24,000 USGS Quadrangle map (**a**), a 1:15,000 airphoto (**b**), and a 1:8,000 airphoto (**c**) for cross-sections 13 (*red*), 15 (*yellow*), and 18 (*green*, Santi 1988)

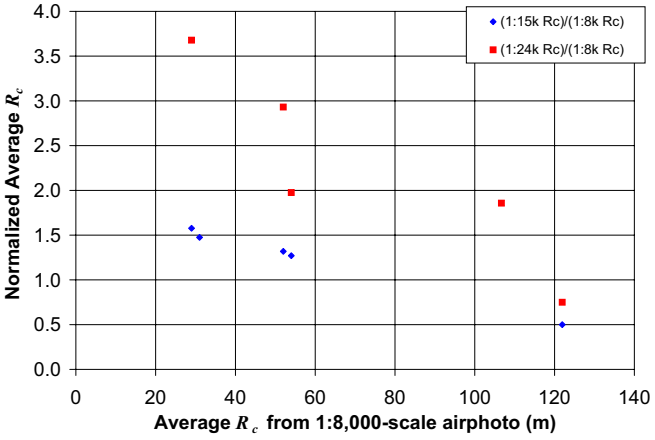

Fig. 7 Normalized average radii of curvature versus average radii of curvature estimated from the 1:8,000-scale airphoto

Discussion

Figure 7 shows that larger radii of curvature resulted from using smaller scale media. This phenomenon is magnified for tighter bends. Thus, an estimated radius of curvature for a natural channel will depend upon the scale of media used for its estimation. To obtain the best definition of a bend's radius of curvature, the largest scale, highest resolution media available should be used.

Variations in back-calculated velocity at different locations along a channel

Methods

In order to investigate the consistency of velocities back-calculated by Eq. 1 at various locations within a reach of channel, velocities were back-calculated from 21 cross-sections along tributary 5 in Santaquin, Utah (McDonald and Giraud 2002). The cross-section locations are shown in Fig. 8.

At each cross-section location, circles were overlaid upon the channel in radii increments of 15 m in order to estimate the maximum and minimum probable radii of curvature. The super-elevation height and flow width were obtained from slope profiler measurements of each cross-section. The position of the debris flow surface at each cross-section was estimated based on either deposit or scour. At cross-sections that had levees or muddy veneer deposits on both sides of the channel, the surface of the flow was assumed to have extended linearly between the two deposits. At cross-sections that did not have debris flow deposits, the surface of the flow was assumed to have extended linearly between the highest debris flow scour on each side of the channel.

Due to the fact that the highest positions of deposit or scour may not necessarily coincide with x, y coordinates of the slope-profiler-obtained cross-sections, reasonable error ranges were applied to the cross-sections based on the expected accuracy of the measurement method. Error ranges of ±0.3 m were applied to the measured flow widths and ±0.1 m were applied to the bank heights. At each cross-section, Eq. 1 (with k=1) was used with the identified ranges of radii of curvature, bank height, and flow width to calculate a range of velocities.

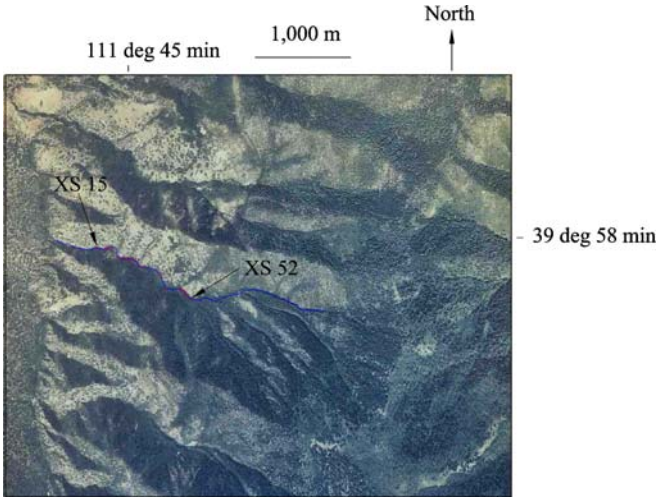

Fig. 8 Locations of cross-sections 15 through 52 in Tributary 5, Santaquin, Utah (McDonald and Giraud 2002)

Results

Figure 9 shows the calculated ranges of velocities for each of the cross-sections shown in Fig. 8. The data points in the interiors of the error bars represent the velocities calculated using the measured bank heights and flow widths and the mean radii of curvature for each cross-section. The extents of the error bars represent the velocities calculated when the error ranges discussed above were applied to the flow widths and bank heights, and radii of curvature were varied between the maximum and minimum ones identified for each cross-section. Negative velocities are reported for cross-sections where scour or deposits were higher on the inside of the curve. This occurrence is explained in the following section.

Discussion

Figure 9 shows that a back-calculated velocity is dependent upon the analyzed location within a channel. Although many cross-sections consistently produced back-calculated velocities in the range of 5 to 15 m/s, others resulted in velocities less than 5 m/s. Taking into account the velocity ranges indicated by the error bars and also the variations between different locations along this reach of channel, a large range of velocities could conceivably be back-calculated from this event.

The anomalously high velocities in Fig. 9 may be attributed to splashing on the outside of a bend; splash marks may have been incorrectly identified as the maximum height of the flow. The presence of deposits being higher on the inside of the bend may be attributed to flow momentum inherited from upstream and interaction with the walls of the bend. In a non-uniform bend, flow may strike the outside wall of the channel and reflect back to the inside rather than gradually superelevating around the bend (T. C. Pierson, 11 December 2006, personal communication).

The presence of deposits being higher on the inside of the bend may also be attributed to supercritical flow. During supercritical flow, superelevation effects can be cancelled if a maximum cross-wave height occurs on the inside of the bend (Pierson 1985). Figure 10 shows a plot of flow velocity versus flow depth for several debris flows. These data were obtained from velocities and corresponding flow depths published by Arattano et al. (1997), Jackson et al. (1989), Jan et al. (2000), Jordan (1994), McArdell et al. (2003), Santi (1988), and Tropeano et al. (2003).

Figure 10 shows that many combinations of debris flow depth and velocity from the technical literature indicate supercritical flow conditions. The forced vortex equation (Eq. 1) assumes subcritical flow (Chow 1959). In order to back-calculate a velocity from supercritical flow, a single cross-section cannot be analyzed. Rather, the effective superelevation height must be measured between inside and outside cross-wave maxima (Pierson 1985).

Lab versus field material properties

Methods

A database of Bingham properties (viscosity and yield strength) was developed from data in the technical literature to investigate the feasibility of using laboratory-measured rheological properties for debris flow velocity predictions in equations such as Eq. 5. Data were divided into two groups: those measured from laboratory tests and those back-calculated from field debris flow events. Laboratory-measured data were obtained from Hamilton and Zhang (1997), Johnson and Martosudarmo (1997), Locat (1997), and Soule (2006). Back-calculated values from field events were

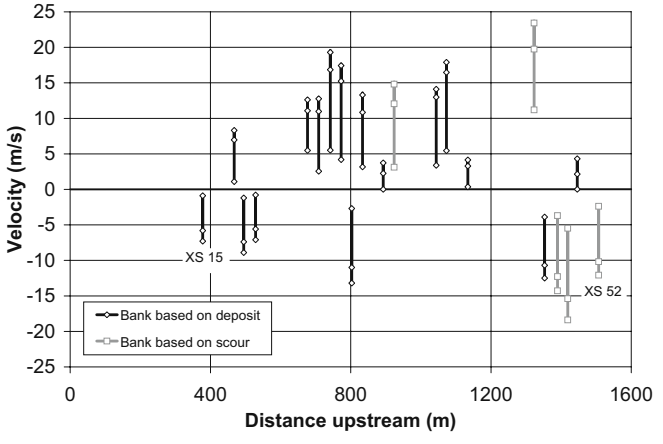

Fig. 9 Back-calculated velocities for cross-sections 15 through 52 in Tributary 5, Santaquin, Utah (McDonald and Giraud 2002). Negative velocities are reported for cross-sections where scour or deposits were higher on the inside of the curve

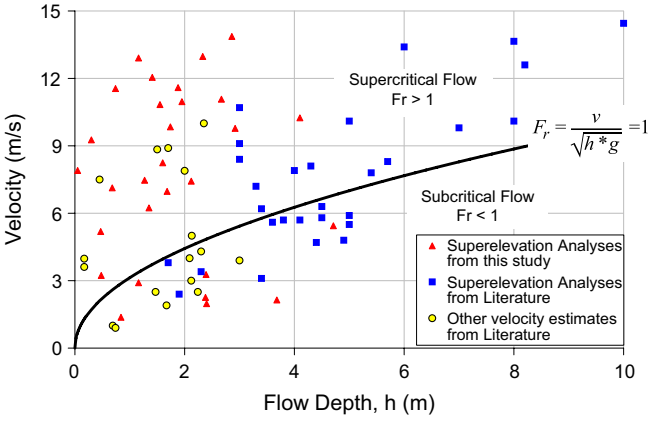

Fig. 10 Debris flow velocity versus flow depth. Many combinations indicate supercritical flow

obtained from Bertolo and Wieczorek (2005), Hungr et al. (1984), Johnson (1984), Jordan (1994), Marina and Giuseppe (2007), Rickenmann and Koch (1997), and Soule (2006).

Results

A plot of Bingham properties (viscosity and yield strength) obtained from laboratory tests and back-calculated from field debris flow events is shown in Fig. 11. Field values that are plotted along each axis did not have corresponding values of the other property reported. Individual data points from Soule (2006) were too numerous to plot, but the extents of his data are represented by the outlined rectangle.

Discussion

Figure 11 shows that two distinct populations of Bingham properties exist between those measured from laboratory tests and those back-calculated from field events. Yield strengths back-calculated from field events vary by nearly an order of magnitude on either side of the generalized estimate of 3,000 Pa*s of Hungr et al. (1984). Higher apparent Bingham properties obtained from field events are presumably due to large-particle frictional interactions, which cannot be measured in laboratory-scale specimens. The presence of this frictional resistance indicates that the back-calculated field events would be more appropriately represented by a Coulomb frictional model than a Bingham model (Iverson 2003) and confirms Major and Iverson's (1999) belief that debris strength cannot be inferred from deposit thickness. Since laboratory-obtained rheological properties are not representative of field-scale debris flow behavior, these values could not be used for velocity predictions. It may be possible to use apparent Bingham properties calibrated from field-scale events to predict the velocities of similar events, although a Bingham model may not be the most physically accurate choice.

Flow trends within channels

Methods

A database of estimated debris flow velocities at different positions within channels was developed from the technical literature. Data were obtained from the following sources: Arattano (2003), Bertolo and Wieczorek (2005), Curry (1966), DeGraff (1997), Jackson (1979), Jackson et al. (1989), Jakob et al. (1997, 2000), Johnson (1984), Meyer and Wells (1997), Meyer et al. (2001), Nasmith and Mercer (1979), and Santi (1988). Debris flow velocity was plotted versus the distance upstream of the fan for each data point.

Much of these velocity data, and other data that will be used in the subsequent section, were back-calculations from superelevations by the original investigators. Although this paper has reported several difficulties with the back-calculation of velocities from superelevations, these are the best data available. These velocities fall within the typical range for debris flows as defined by Lorenzini and Mazza (2004) and are also within the range of debris flow velocities obtained by more certain methods such as instrumentation (e.g., Arattano and Grattoni 2000; Genevois et al. 2000; Suwa et al. 2003), video surveillance (e.g., Arattano and Grattoni 2000; Genevois et al. 2000; Zhang and Chen 2003), or eyewitnesses (e.g., Hungr et al. 1984; Jackson 1979). Flow depths reported within the original references indicate that approximately half of these velocity data were collected from subcritical flows.

Based on the form of Eq. 4, channel slope and flow depth were identified as being two easily measured factors expected to correlate to measured velocity. The channel slope and flow depth were identified for each measured cross-section in several of the examined basins that produced fire-related debris flows. The basins used for analysis were tributaries 2, 3, 4, 5, and 6 in Utah (Gartner 2005; McDonald and Giraud 2002); Elkhorn, Kroeger, and Woodard in Colorado (Gartner 2005); and Devore, El Capitan I, Lytle Creek W, Waterman N North, and Water Tank in California (Gartner 2005). The data obtained from these basins (Gartner 2005) do not allow for the differentiation between instantaneous flow depths and the maximum depth of scour. Thus, the flow depth used for this analysis was the depth from the top of debris flow scour or deposit to the bottom of the scoured channel, which may be greater than any instantaneous flow depth. For each basin, the value h^2S at each cross-section was analyzed versus the distance upstream of the fan, where h is the flow depth and S is the sine of the channel slope. The decision to use h^2S was based on empirical data, which will be shown in a subsequent section. However, these exponential powers of flow depth and channel slope are identical to those used in Newtonian laminar flow and Bingham laminar flow equations (Lo 2000) and are also proportional to the shear force within a steady, uniform, viscous flow (Savage and Smith 1986).

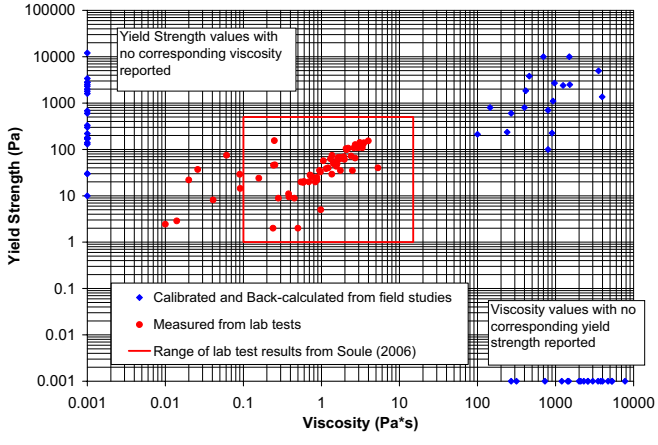

Fig. 11 Bingham properties (viscosity and yield strength) obtained from laboratory tests and field back-calculations

Results

Velocity estimates had been made at numerous points along the travel path for three debris flow events in the literature: Cathedral Gulch 1984 (Jackson et al. 1989), Hummingbird Creek (Jakob et al. 2000), and Layton, Utah (Santi 1988). Velocity trends for these three events are shown in Fig. 12. The trends for these three events show that velocities were generally consistent along the length of the channel.

Figure 13 shows a plot of all the data from the technical literature for estimated debris flow velocities versus the distance upstream of the alluvial fan. These data include those from Fig. 12 in addition to data from debris flows for which only one or two velocity measurements were made. These data show that a wider range of velocities have been reported near alluvial fans than farther upstream in channels.

The h^2S data measured from fire-related debris flows (Santi et al. 2006) were statistically analyzed for any trends along the lengths of the debris flow paths. Figure 14 shows an example of h^2S values

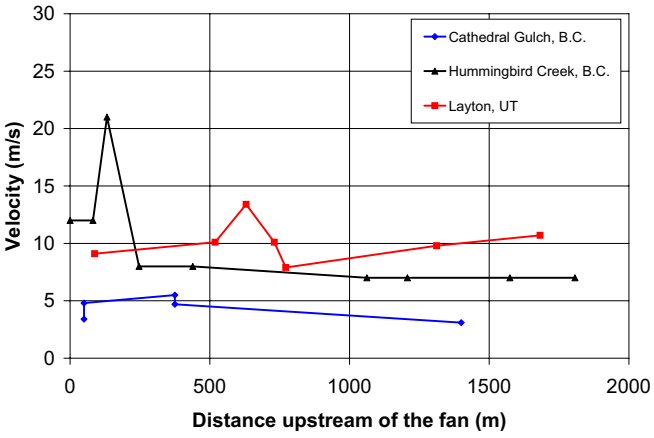

Fig. 12 Debris flow velocity estimations versus distance upstream of the fan for individual events

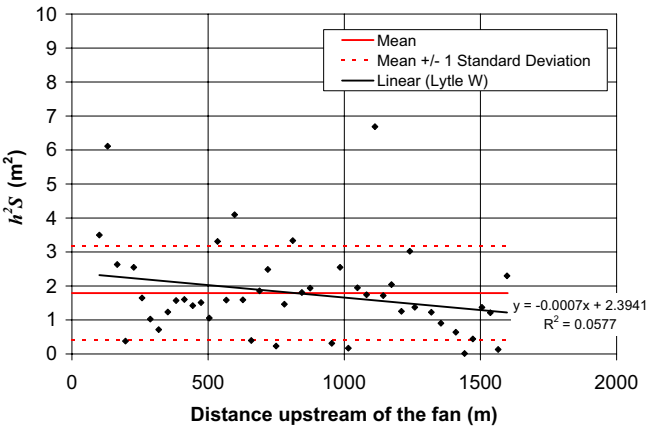

Fig. 14 Example of h^2S versus distance upstream of the fan for Lytle Creek W (Gartner 2005), where h is the flow depth and S is the sine of the channel angle

from each cross-section of Lytle Creek W, along with their mean, standard deviation, and regression results. A summary of these data from all the analyzed basins is shown in Table 2. Also shown in Table 2 are the P values obtained from regressions of h^2S versus distance upstream for each analyzed basin.

Discussion

The results in Fig. 12 show that velocities were approximately constant along the length of the flow path for the three events shown. Although some data points show localized deviations, velocity is generally consistent along these flow paths. These results contradict Pierson (1985) who found that velocities decreased along the lengths of flow paths for the Pine Creek and Muddy River lahars. Comparing these lahars to the events shown in Fig. 12 would be questionable, though, due to the larger magnitude (1.4×10^7 m^3) and initiation mode (pyroclastic surge) of the lahars.

The results in Fig. 12, which show uniform velocities along flow paths, were obtained from a few choice locations along the channel. The results in Fig. 9, which show a wide range of back-calculated velocities along the flow path, were obtained from a much denser sampling of bends along the channel length. Therefore, not all channel bends will be appropriate for super-elevation calculations, and care must be taken when choosing bends to analyze.

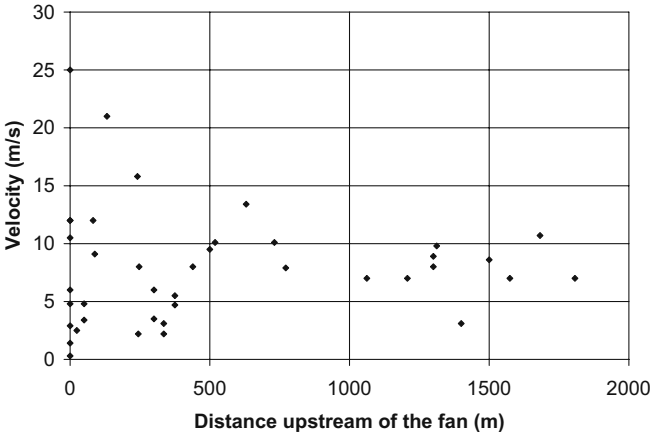

Fig. 13 Debris flow velocity estimations versus distance upstream of the fan

Figure 13 shows that for all the data from the technical literature, a wider range of velocities are reported near alluvial fans than farther upstream in channels. We interpret this not to mean that velocities become more variable near alluvial fans, but rather that a wider range of events have been examined near the mouths of channels. In Fig. 13, data presented within the first 500 m from the fan were obtained from 14 different debris flow events, while data presented greater than 500 m from the fan were obtained from only six different events reported by five sources. The wide range of velocities reported near the fan in Fig. 13 may also be caused by decreasing velocities due to deposition or the inconsistency of velocity estimation methods.

The high P values on the regressions in Table 2 indicate that for all but two basins, the regressions are not statistically significant at a significance level of 0.05. Therefore, it would be concluded that the mean is just as good a predictor of h^2S as is the regression, and h^2S is constant along the travel path. This is caused by the simultaneous decrease in channel slope along the flow path as bulked material increases the flow depth. For the two basins with statistically significant regressions (tributary 2 and Woodard), the practical significance of these regressions will be discussed in a subsequent section.

The data from the basins listed in Table 2 were obtained primarily from modest-sized debris flow events, with magnitudes less than 20,000 m^3 (size classes 3 and 4, Jakob 2005). For every event other than Devore, the mean h^2S value was less than or equal to 2.5 m^2, and the channel had been scoured to bedrock over much of its length. The magnitude of this h^2S value will be put into perspective in a subsequent section. The constancy of h^2S values along the travel paths of these fire-related debris flows is attributed to the presence of shallow bedrock, which limits the potential depth of scour. Thus, the event volume, peak flow, and flow depth are also finite.

Devore was the only analyzed basin with a mean h^2S value greater than 3 m^2. Although no statistically significant trend was observed between h^2S and the channel position for Devore, this event did exhibit highly random h^2S values and a high depth of flow overall. We attribute this to the abundance of material available for mobilization within the channel, since Devore Canyon

Table 2 Summary of h^2S versus upstream distance data for all analyzed basins

			Regression results				*P* values			
Basin	Mean of h^2S (m^2)	Standard deviation of h^2S (m^2)	Slope (m) × 10^{-5}	Slope SE (m) × 10^{-5}	Intercept (m^2)	Intercept SE[a] (m^2)	Intercept	Regression	Number	Channel length (m)
Tributary 2	0.87	0.92	55	17	0.18	0.24	0.46	0.00	63	2,300
Tributary 3	0.72	0.80	16	9.4	0.45	0.18	0.02	0.09	73	3,400
Tributary 4	0.67	0.95	7.0	12	0.56	0.22	0.02	0.56	68	3,200
Tributary 5	1.7	1.8	−74	57	2.3	0.53	0.00	0.20	46	1,500
Tributary 6	0.85	0.88	22	18	0.59	0.24	0.02	0.21	51	2,400
Elkhorn	2.5	3.5	−260	140	4.2	1.1	0.00	0.07	41	1,300
Kroeger	0.19	0.18	−4.2	3.3	0.25	0.06	0.00	0.21	41	3,000
Woodard	1.0	2.4	−190	56	3.2	0.71	0.00	0.00	48	2,000
Devore	4.6	3.3	120	110	3.8	0.87	0.00	0.29	47	1,400
El Capitan I	1.4	1.1	−39	84	1.56	0.44	0.00	0.64	29	890
Lytle Creek W	1.8	1.4	−74	45	2.4	0.42	0.00	0.11	46	1,600
Waterman N North	0.60	0.49	−99	66	0.95	0.26	0.00	0.16	17	600
Water tank	2.1	2.3	490	410	0.84	1.1	0.47	0.25	21	430

SE standard error

is located near the convergence of several faults (Dibblee 2003a, b). Field observations showed channel incision of up to 2 m into stored colluvium in the channel of Devore Canyon.

We would expect landslide-initiated debris flows to show similar trends to the analyzed fire-related flows, but to have higher h^2S values due to the volume of the initiating event. Some basins in Table 2 have standard deviations of the h^2S values that are larger than the mean value; this is attributed to the presence of a few anomalously deeply scoured cross-sections in a channel with an otherwise low mean h^2S value.

Since velocity and h^2S are both approximately constant along the paths of the analyzed debris flows, it may be possible to obtain a preliminary velocity estimate from the channel slope and the expected depth of flow. This estimated velocity would be applicable along the entire length of channel.

Velocity versus h^2S

Methods

A database was developed from the technical literature for locations where an estimated velocity, flow depth, and channel slope were all reported. Data were obtained from the following sources: Jackson et al. (1989), Jordan (1994), Santi (1988), and Tropeano et al. (2003). These data are from landslide-initiated debris flows in British Columbia, Utah, and Italy. Although these velocities were back-calculated from superelevations, we again consider them valid for the same reasons presented in the previous section. Statistical analyses were performed to correlate velocity to h^2S. A larger dataset would have been desirable, but reports in the technical literature of debris flow velocity, flow depth, and channel slope at a single location were rare.

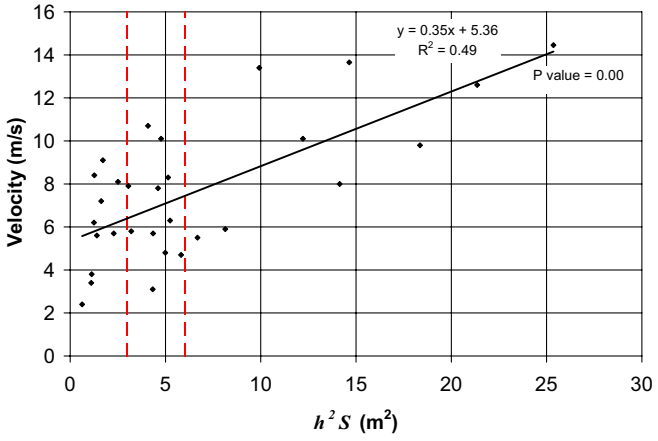

Fig. 15 Velocity versus h^2S. *Dashed vertical lines* are at h^2S equal to 3 and 6 m^2

Results

Figure 15 shows a plot of velocity versus h^2S, along with the best-fit regression line to the data. The standard errors of the regression line's slope and intercept are 0.06 and 0.61, respectively. The residuals from this regression are homoscedastic and the normal probability plot of the residuals is reasonably linear. The vertical lines in Fig. 15 divide the data into three near-equal subsets at h^2S values of 3 and 6 m^2. The statistical distribution of the data within each subset is summarized in Table 3.

Discussion

The R^2 value in Fig. 15 shows that h^2S explains approximately half of the scatter within the dataset. The other half of the scatter is likely due to differences in material properties and channel characteristics between the events in the dataset. These additional factors (coefficient *a* from Eq. 4) are approximately incorporated into the slope of the best-fit regression line shown in Fig. 15, which are too varied and difficult to characterize and quantify to justify attempts to

Table 3 Summary of velocity versus h^2S data

	$h^2S<3$ m^2 (m/s)	3 $m^2<h^2S<6$ m^2 (m/s)	6 $m^2<h^2S$ (m/s)
Mean − 1 SD	3.7	4.5	7.0
Mean	6.0	6.8	10.4
Mean + 1 SD	8.3	9.1	13.8
Mean + 2 SD	10.6	11.4	17.2

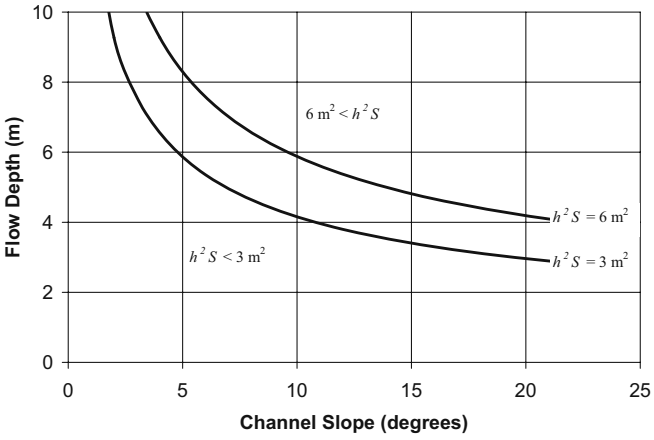

Fig. 16 Flow depth and channel slope combinations at the h^2S category boundaries

include them in the correlation to predict a preliminary velocity. The low P value indicates that the regression is statistically significant; the velocities within the dataset do increase with increasing values of h^2S, and h^2S is a better predictor of velocity than is the mean of the dataset. The results summary shown in Table 3 is based on a limited amount of available data, and considerable scatter exists within the data shown in Fig. 15. However, this method shows promise of h^2S being a predictor of debris flow velocity (if the velocities back-calculated from superelevations are correct), and it should be tested with additional data as they become available.

In comparing the h^2S data from Table 2 to the data and analysis reported by Fig. 15 and Table 3, all but one of the analyzed debris flow events from Table 2 would fall within the lowest category of Table 3: $h^2S<3$ m^2. For the two events that had statistically significant regressions (Table 2, tributary 2 and Woodard), deviations along the channel are still contained within the category $h^2S<3$ m^2. Devore would fall within the middle category, and no analyzed events from Table 2 had h^2S values larger than 6 m^2.

Figure 16 shows the flow depth and channel slope combinations at the h^2S category boundaries shown in Fig. 15 and Table 3. Modest-sized flows will have h^2S values less than 3 m^2, and only very large flows will have h^2S values greater than 6 m^2.

A velocity may be estimated from Table 3 for use in preliminary designs. A maximum possible flow depth, h, may be estimated as the height from bedrock to the top of the channel banks. This estimate conservatively assumes that during a debris flow, the channel has been scoured down to bedrock and the channel is flowing full. An increase in flow depth above the height of the channel banks will cause material to spill over and deposit due to lack of confinement, effectively limiting the maximum potential flow depth. However, for long-duration debris flows with multiple surges, the maximum instantaneous flow depth may be less than this maximum possible depth. Alternatively, the high flow marks from previous debris flows could be used to estimate a flow depth for the prediction of the velocities of similar-sized events. This method would be required for deeply incised canyons that do not contain channel banks to limit the maximum height of flow.

Combinations of flow depth and channel slope other than h^2S were preliminarily investigated as being predictors of velocity, as were other channel and material characteristics. Based on data available within the technical literature, h^2S was found to produce the highest R^2 value of the various combinations of predictors, although other combinations of flow depth and channel slope fit the velocity data similarly (Table 4). Best-fit regression equations obtained from other combinations of flow depth and channel slope are summarized in Table 4.

Summary and conclusions

Back-calculation of velocities for recent debris flows has been shown to be a subjective and problematic process. There is not an absolute value of a radius of curvature for a natural channel's bend, but reasonable approximations may be made. An estimated radius of curvature will vary with the extent of the bend investigated and the scale of the media used. Because of their dependence on this measurement, back-calculated velocities can vary significantly between different analyzed cross-sections. Another significant difficulty with velocity back-calculation is that many debris flow events from the technical literature would be classified as supercritical flows. In these instances, the forced vortex equation (Eq. 1) cannot be applied to an individual cross-section, but rather the superelevation height must be estimated between inside and outside cross-wave maxima.

This paper has identified several difficulties with the use of the forced vortex equation. However, the purpose of this paper has only been to disseminate these difficulties, not to denounce the method entirely. Many experienced researchers have reported back-calculated velocities from superelevations that appear to be reasonable, but the process is not nearly as straightforward as it appears.

Prediction of debris flow velocity at locations where back-calculation is not possible requires information about material properties for use in flow equations. We have shown that two populations of Bingham properties (viscosity and yield strength) exist between those measured from laboratory samples and those back-calculated from field-scale debris flows. This indicates that a Bingham model would not be physically appropriate for friction-dominated debris flows, which are flows containing large particles. Therefore, laboratory-obtained properties, which are generally derived from only the finer fraction of debris samples, should not

Table 4 Analysis results using other combinations of flow depth and channel slope

Flow model	Form of flow depth (h) and channel slope (S)	Reference	Best-fit regression equation[a]	R^2
Dilatant	$h^{3/2}S^{1/2}$	Hungr et al. (1984); Lo (2000)	$v = 0.55\left(h^{3/2}S^{1/2}\right) + 4.59$	0.47
Newtonian turbulent (Manning)	$h^{2/3}S^{1/2}$	Lo (2000); Rickenmann (1999)	$v = 4.47\left(h^{2/3}S^{1/2}\right) + 1.71$	0.44
Newtonian turbulent (Chézy)	$h^{1/2}S^{1/2}$	Rickenmann (1999)	$v = 6.53\left(h^{1/2}S^{1/2}\right) + 1.03$	0.37
Empirical	$h^{2/3}S^{1/5}$	Lo (2000)	$v = 3.32\left(h^{2/3}S^{1/5}\right) + 0.70$	0.47
Empirical	$h^{0.3}S^{1/2}$	Rickenmann (1999)	$v = 8.90\left(h^{0.3}S^{1/2}\right) + 1.06$	0.24

[a]With flow depth in meters and velocity in m/s.

be used for field-scale velocity predictions. However, reasonable velocity estimates may be obtained if back-calculated apparent Bingham properties are used.

Flow velocity and h^2S both tentatively appear to be rather consistent along the length of a debris flow path. A preliminary debris flow velocity prediction can be made from a channel's slope and the expected depth of flow by using Table 3, if the back-calculated velocity data presented in Fig. 15 are assumed to be correct. The maximum depth of flow would extend from bedrock to the loss of confinement at the top of the channel banks. Although the relationship between h^2S and velocity is based on only a modest dataset, it appears to be a worthwhile estimation method that avoids the difficulties of other debris flow velocity estimation methods. The validity of this method should continue to be assessed as additional data become available.

Acknowledgments

This work has been funded by the US Department of Education through a Graduate Assistance in Areas of National Need (GAANN) Fellowship, award #P200A060133. Thanks to Richard Giraud from the Utah Geological Survey for providing airphotos and to Ron Allingham for AutoCAD assistance. Also thanks to Victor deWolfe, Joe Gartner, Morgan McArthur, and Nate Soule for the measurement of many of the cross-sections used in this study. Joe Gartner, Jason Kean, and two anonymous reviewers provided helpful comments on an earlier draft of this paper.

References

Apmann RP (1973) Estimating discharge from superelevation in bends. J Hydraul Div 99:65–79

Arattano M (2003) Monitoring the presence of the debris-flow front and its velocity through ground vibration detectors. In: Rickenmann D, Chen C-L (eds) Debris-flow hazards mitigation: mechanics, prediction, and assessment. Proceedings of the third international conference. Millpress, Rotterdam, pp 719–730

Arattano M, Grattoni P (2000) Using a fixed video camera to measure debris-flow surface velocity. In: Wieczorek GF, Naeser ND (eds) Debris-flow hazards mitigation: mechanics, prediction, and assessment. Proceedings of the second international conference. AA Balkema, Rotterdam, pp 273–281

Arattano M, Deganutti AM, Marchi L (1997) Debris flow monitoring activities in an instrumented watershed on the Italian Alps. In: Chen C-L (ed) Debris-flow hazards mitigation: mechanics, prediction, and assessment. Proceedings of the first international conference. ASCE, New York, pp 506–515

Bertolo P, Wieczorek GF (2005) Calibration of numerical models for small debris flows in Yosemite Valley, California, USA. Nat Hazards Earth Syst Sci 5:993–1001

Chen C-L (1987) Comprehensive review of debris flow modeling concepts in Japan. In: Costa JE, Wieczorek GF (eds) Reviews in engineering geology, vol VII. Debris flows/avalanches: process, recognition, and mitigation. The Geological Society of America, Boulder, CO, pp 13–29

Chou HT, Liao WM, Lin ML (2000) Landslide induced debris-flow at a dump site. In: Wieczorek GF, Naeser ND (eds) Debris-flow hazards mitigation: mechanics, prediction, and assessment. Proceedings of the second international conference. AA Balkema, Rotterdam, pp 157–160

Chow VT (1959) Open-channel hydraulics. McGraw-Hill, New York

Costa JE (1984) Physical geomorphology of debris flows. In: Costa JE, Fleisher PJ (eds) Developments and applications of geomorphology. Springer, Berlin, pp 268–317

Cui P, Chen X, Waqng Y, Hu K, Li Y (2005) Jiangjia Ravine debris flows in south-western China. In: Jakob M, Hungr O (eds) Debris-flow hazards and related phenomena. Praxis, Chichester, pp 565–594

Curry RR (1966) Observation of alpine mudflows in the Tenmile Range, central Colorado. Geol Soc Amer Bull 77:771–776

DeGraff JV (1997) Geologic investigation of the Pilot Ridge debris flow, Groveland Ranger District, Stanislaus National Forest. United States Department of Agriculture Forest Service FS-6200-7 (10/73)

Dibblee TW Jr (2003a) Geologic map of the Cajon Quadrangle, San Bernardino County, California. Dibblee geology center map #DF-104. Santa Barbara Museum of Natural History, Santa Barbara, California

Dibblee TW Jr (2003b) Geologic map of the Devore Quadrangle, San Bernardino County, California. Dibblee geology center map #DF-105. Santa Barbara Museum of Natural History, Santa Barbara, California

Gartner JE (2005) Relations between wildfire related debris-flow volumes and basin morphology, burn severity, material properties and triggering storm rainfall. Master of Arts thesis, University of Colorado Department of Geography

Genevois R, Tecca PR, Berti M, Simoni A (2000) Debris-flows in the dolomites: experimental data from a monitoring system. In: Wieczorek GF, Naeser ND (eds) Debris-flow hazards mitigation: mechanics, prediction, and assessment. Proceedings of the second international conference. AA Balkema, Rotterdam, pp 283–291

Hamilton D, Zhang S (1997) Velocity profile assessment for debris flow hazards. In: Chen C-L (ed) Debris-flow hazards mitigation: mechanics, prediction, and assessment. Proceedings of the first international conference. ASCE, New York, pp 474–483

Henderson FM (1966) Open channel flow. Macmillan, New York

Hungr O, Morgan GC, Kellerhals R (1984) Quantitative analysis of debris torrent hazards for design of remedial measures. Can Geotech J 21:663–677

Iverson RM (1997) The physics of debris flows. Rev Geophys 35:245–296

Iverson RM (2003) The debris-flow rheology myth. In: Rickenmann D, Chen C-L (eds) Debris-flow hazards mitigation: mechanics, prediction, and assessment. Proceedings of the third international conference. Millpress, Rotterdam, pp 303–314

Iverson RM, LaHusen RG, Major JJ, Zimmerman CL (1994) Debris flow against obstacles and bends: dynamics and deposits. EOS Trans Am Geophys Union 75:274

Jackson LE Jr (1979) A catastrophic glacial outburst flood (jökulhlaup) mechanism for debris flow generation at the Spiral Tunnels, Kicking Horse River basin, British Columbia. Can Geotech J 16:806–813

Jackson LE Jr, Hungr O, Gardner JS, Mackay C (1989) Cathedral Mountain debris flows, Canada. Bull Int Assoc Eng Geol 40:35–54

Jakob M (2005) A size classification for debris flows. Eng Geol 79:151–161

Jakob M, Hungr O, Thomson B (1997) Two debris flows with anomalously high magnitude. In: Chen C-L (ed) Debris-flow hazards mitigation: mechanics, prediction, and assessment. Proceedings of the first international conference. ASCE, New York, pp 382–394

Jakob M, Anderson D, Fuller T, Hungr O, Ayotte D (2000) An unusually large debris flow at Hummingbird Creek, Mara Lake, British Columbia. Can Geotech J 37:1109–1125

Jan CD, Wang YY, Han WL (2000) Resistance reduction of debris-flow due to air entrainment. In: Wieczorek GF, Naeser ND (eds) Debris-flow hazards mitigation: mechanics, prediction, and assessment. Proceedings of the second international conference. AA Balkema, Rotterdam, pp 369–372

Johnson AM (1984) Debris flow. In: Brunsden D, Prior DB (eds) Slope instability. Wiley, Chichester, pp 257–361

Johnson AM, Martosudarmo SY (1997) Discrimination between inertial and macro-viscous flows of fine-grained debris with a rolling-sleeve viscometer. In: Chen C-L (ed) Debris-flow hazards mitigation: mechanics, prediction, and assessment. Proceedings of the first international conference. ASCE, New York, pp 229–238

Jordan RP (1994) Debris flows in the Southern Coast Mountains, British Columbia: dynamic behaviour and physical properties. Doctor of Philosophy thesis, The University of British Columbia

Keaton JR, DeGraff JV (1996) Surface observation and geologic mapping. In: Turner AK, Schuster RL (eds) Landslides investigation and mitigation. Special Report 247, Transportation Research Board, National Research Council, Washington, pp 178–230

Lo DOK (2000) Review of natural terrain landslide debris-resisting barrier design. GEO Report No. 104, Geotechnical Engineering Office, Civil Engineering Department, The Government of Hong Kong Special Administrative Region

Locat J (1997) Normalized rheological behaviour of fine muds and their flow properties in a pseudoplastic regime. In: Chen C-L (ed) Debris-flow hazards mitigation: mechanics, prediction, and assessment. Proceedings of the first international conference. ASCE, New York, pp 260–269

Lorenzini G, Mazza N (2004) Debris flow phenomenology and rheological modeling. WIT Press, Southampton

Major JJ, Iverson RM (1999) Debris-flow deposition: effects of pore-fluid pressure and friction concentrated at flow margins. GSA Bull 111:1424–1434

Marina P, Giuseppe S (2007) The runout of debris flows: application of two numerical models and comparison of results. Proceedings of the first North American landslide conference, Vail, Colorado, 3–8 June 2007 (compact disk)

McArdell BW, Zanuttigh B, Lamberti A, Rickenmann D (2003) Systematic comparison of debris-flow laws at the Illgraben torrent, Switzerland. In: Rickenmann D, Chen C-L (eds) Debris-flow hazards mitigation: mechanics, prediction, and assessment. Proceedings of the third international conference. Millpress, Rotterdam, pp 647–657

McClung DM (2001) Superelevation of flowing avalanches around curved channel bends. J Geophys Res 106:16,489–16,498
McDonald GN, Giraud RE (2002) September 12, 2002, fire-related debris flows east of Santaquin and Spring Lake, Utah County, Utah. Technical Report 02-09, Utah Geological Survey, Salt Lake City, Utah
Meyer GA, Wells SG (1997) Fire-related sedimentation events on alluvial fans, Yellowstone National Park, U.S.A. J Sediment Res 67:776–791
Meyer GA, Pierce JL, Wood SH, Jull AJT (2001) Fire, storms, and erosional events in the Idaho batholith. Hydrol Process 15:3025–3038
Nasmith HW, Mercer AG (1979) Design of dykes to protect against debris flows at Port Alice, British Columbia. Can Geotech J 16:748–757
O'Brien JS (1986) Physical processes, rheology and modeling of mud flows. Doctor of Philosophy dissertation, Colorado State University
Pashias N, Boger DV (1996) A fifty cent rheometer for yield stress measurement. J Rheol 40:1179–1189
Pierson TC (1985) Initiation and flow behavior of the 1980 Pine Creek and Muddy River lahars, Mount St. Helens, Washington. Geol Soc Amer Bull 96:1056–1069
Pierson TC, Costa JE (1987) A rheologic classification of subaerial sediment-water flows. In: Costa JE, Wieczorek GF (eds) Reviews in engineering geology, vol VII. Debris flows/avalanches: process, recognition, and mitigation. The Geological Society of America, Boulder, CO, pp 1–12
Reneau SL, Dietrich WE (1987) The importance of hollows in debris flow studies; examples from Marin County, California. In: Costa JE, Wieczorek GF (eds) Reviews in engineering geology, vol VII. Debris flows/avalanches: process, recognition, and mitigation. The Geological Society of America, Boulder, CO, pp 165–180
Rickenmann D (1999) Empirical relationships for debris flows. Nat Hazards 19:47–77
Rickenmann D, Koch T (1997) Comparison of debris flow modelling approaches. In: Chen C-L (ed) Debris-flow hazards mitigation: mechanics, prediction, and assessment. Proceedings of the first international conference. ASCE, New York, pp 576–585
Santi PM (1988) The kinematics of debris flow transport down a canyon. Master of Science in Geology Thesis, Texas A&M University
Santi PM, Higgins JD, Cannon SH, DeGraff JV (2006) Evaluation of post-wildfire debris flow mitigation methods and development of decision-support tools. Final Report to the Joint Fire Science Program, JFSP Contract 03-1-4-14. Also at http://www.firescience.gov/projects/03-1-4-14/03-1-4-14_final_report.pdf
Savage WZ, Smith WK (1986) A model for the plastic flow of landslides. US Geological Survey Professional Paper 1385, United States Government Printing Office, Washington, DC
Soule NC (2006) The influence of coarse material on the yield strength and viscosity of debris flows. Master of Science in Geological Engineering Thesis, Colorado School of Mines
Suwa H, Yamakoshi T (2000) Estimation of debris-flow motion by field surveys. In: Wieczorek GF, Naeser ND (eds) Debris-flow hazards mitigation: mechanics, prediction, and assessment. Proceedings of the second international conference. AA Balkema, Rotterdam, pp 293–299
Suwa H, Akamatsu J, Nagai Y (2003) Energy radiation by elastic waves from debris flows. In: Rickenmann D, Chen C-L (eds) Debris-flow hazards mitigation: mechanics, prediction, and assessment. Proceedings of the third international conference. Millpress, Rotterdam, pp 895–904
Thomas GB Jr, Finney RL (1984) Calculus and analytic geometry. Addison-Wesley, Reading, Massachusetts
Tropeano D, Turconi L, Rosso M, Cavallo C (2003) The October 15, 2000 debris flow in the Bioley torrent, Fenis, Aosta valley, Italy—damage and processes. In: Rickenmann D, Chen C-L (eds) Debris-flow hazards mitigation: mechanics, prediction, and assessment. Proceedings of the third international conference. Millpress, Rotterdam, pp 1037–1048
VanDine DF (1985) Debris flows and debris torrents in the Southern Canadian Cordillera. Can Geotech J 22:44–68
VanDine DF (1996) Debris flow control structures for forest engineering. British Columbia Ministry of Forests Research Program, Working Paper 08/1996
Williams GP (1986) River meanders and channel size. J Hydrol 88:147–164
Zhang S, Chen J (2003) Measurement of debris-flow surface characteristics through close-range photogrammetry. In: Rickenmann D, Chen C-L (eds) Debris-flow hazards mitigation: mechanics, prediction, and assessment. Proceedings of the third international conference. Millpress, Rotterdam, pp 775–784

A. B. Prochaska (✉) · **P. M. Santi** · **J. D. Higgins**
Department of Geology and Geological Engineering, Colorado School of Mines,
1516 Illinois Street,
Golden, CO 80401, USA
e-mail: adamprochaska@hotmail.com

S. H. Cannon
US Geological Survey,
P.O. Box 25046 Mail Stop 966,
Denver, CO 80225-0046, USA